LETTER

doi:10.1038/nature14290

Monolayer semiconductor nanocavity lasers with ultralow thresholds

Sanfeng Wu[1], Sonia Buckley[2], John R. Schaibley[1], Liefeng Feng[1,3], Jiaqiang Yan[4,5], David G. Mandrus[4,5,6], Fariba Hatami[7], Wang Yao[8], Jelena Vučković[2], Arka Majumdar[9] & Xiaodong Xu[1,10]

Engineering the electromagnetic environment of a nanometre-scale light emitter by use of a photonic cavity can significantly enhance its spontaneous emission rate, through cavity quantum electrodynamics in the Purcell regime. This effect can greatly reduce the lasing threshold of the emitter[1–5], providing a low-threshold laser system with small footprint, low power consumption and ultrafast modulation. An ultralow-threshold nanoscale laser has been successfully developed by embedding quantum dots into a photonic crystal cavity (PCC)[6–8]. However, several challenges impede the practical application of this architecture, including the random positions and compositional fluctuations of the dots[7], extreme difficulty in current injection[8], and lack of compatibility with electronic circuits[7,8]. Here we report a new lasing strategy: an atomically thin crystalline semiconductor—that is, a tungsten diselenide monolayer—is non-destructively and deterministically introduced as a gain medium at the surface of a pre-fabricated PCC. A continuous-wave nanolaser operating in the visible regime is thereby achieved with an optical pumping threshold as low as 27 nanowatts at 130 kelvin, similar to the value achieved in quantum-dot PCC lasers[7]. The key to the lasing action lies in the monolayer nature of the gain medium, which confines direct-gap excitons to within one nanometre of the PCC surface. The surface-gain geometry gives unprecedented accessibility and hence the ability to tailor gain properties via external controls such as electrostatic gating and current injection, enabling electrically pumped operation. Our scheme is scalable and compatible with integrated photonics for on-chip optical communication technologies.

Monolayer transition-metal dichalcogenides (TMDCs) with chemical formula MX_2 (M = W, Mo; X = S, Se, Te; see Fig. 1a for the crystal structure) are the first class of two-dimensional (2D) semiconductors to be discovered that have a direct bandgap in the visible frequency range[9,10]; tightly bound excitons with novel properties are being found in these systems at such frequencies[11–13]. These structurally stable, mechanically strong, electrically

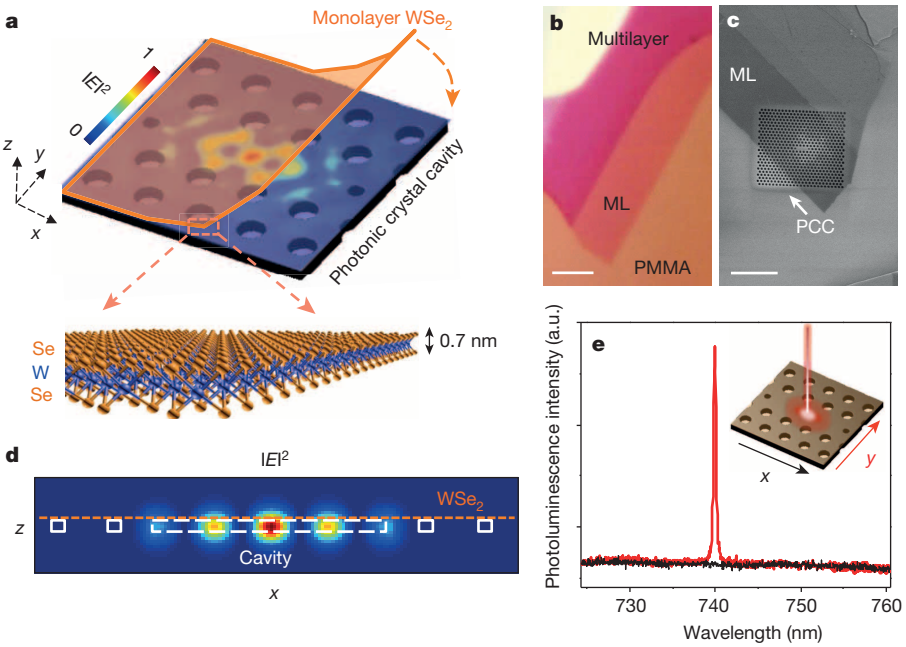

Figure 1 | Hybrid monolayer WSe_2–PCC nanolasers. **a**, Cartoon depiction of our device architecture, where the electric-field profile (in-plane, x–y) of the fundamental cavity mode (pristine cavity before WSe_2 transfer) is embedded as the colour plot. Inset, cartoon of the atomic structure of monolayer WSe_2. **b**, Optical image of monolayer (ML) WSe_2 on PMMA before transfer. **c**, SEM image of the hybrid device. Q-factor is ~8,000 in this cavity before WSe_2 transfer. Scale bars: 3 μm. **d**, Cross-section electric-field intensity ($|E|^2$) profile (x–z) of the fundamental mode; the dashed orange line indicates the ideal position for monolayer WSe_2, the solid white rectangles for air holes, and dashed white lines for the cavity region. **e**, Polarization-resolved photoluminescence spectrum of our device taken at 80 K, showing a completely polarized narrow emission at ~740 nm. Black (red) line corresponds to detected linear polarization in the x (y) direction.

[1]Department of Physics, University of Washington, Seattle, Washington 98195, USA. [2]Ginzton Laboratory, Stanford University, Stanford, California 94305, USA. [3]Department of Applied Physics, Tianjin University, Tianjin 300072, China. [4]Materials Science and Technology Division, Oak Ridge National Laboratory, Oak Ridge, Tennessee 37831, USA. [5]Department of Materials Science and Engineering, University of Tennessee, Knoxville, Tennessee 37996, USA. [6]Department of Physics and Astronomy, University of Tennessee, Knoxville, Tennessee 37996, USA. [7]Department of Physics, Humboldt University, D-12489 Berlin, Germany. [8]Department of Physics and Center of Theoretical and Computational Physics, University of Hong Kong, Hong Kong, China. [9]Department of Electrical Engineering, University of Washington, Seattle, Washington 98195, USA. [10]Department of Material Science and Engineering, University of Washington, Seattle, Washington 98195, USA.

tunable and optically active materials have generated substantial interest in the scientific community owing to their potential for use in 'spin-valleytronics'[14,15], field effect transistors[16], light emitting diodes[17–19], solar cells[20] and photodetectors[21], thereby possibly expanding the science and device applications of 2D crystals.

Here we demonstrate the first nanoscale laser system based on 2D quantum materials, harnessing the unique advantages of atomically thin crystals for coherent light generation. In our architecture, monolayer tungsten diselenide (WSe_2), as seen in the optical image in Fig. 1b, is selected as the gain medium owing to its desirable bandwidth and relatively high photoluminescence quantum yield compared to other TMDC monolayers. The monolayer is coupled to a prefabricated PCC on a gallium phosphide (GaP) thin membrane[22] that is transparent to WSe_2 emission (see Fig. 1a and Methods). An L3 type of PCC is employed[23], in which three neighbouring holes in a linear arrangement are missing, as shown in the scanning electron microscopy (SEM) image in Fig. 1c. The PCC is carefully designed; the mode with the highest quality factor (Q-factor) is resonant around 740 nm, which is in the band of the monolayer photoluminescence.

Controlled spontaneous emission was recently demonstrated in monolayer semiconductors, where low Q-factor (~300) PCCs[24,25] or distributed Bragg reflectors[26] were used. In our devices, the as-fabricated PCCs have Q-factors of about 10^4 (Extended Data Fig. 1), representing an improvement of ~30 times. This results in a significant improvement of the Purcell factor[24,25] (see Methods), which is crucial for lasing. To achieve such a high Q-factor in the visible region, we use a 125-nm-thick membrane (see Methods), which is 55 nm thinner than our previously reported low-Q cavity where no lasing behaviour was observed[25]. This design significantly improves the cavity Q-factors, owing to an optimal thickness-to-lattice-constant ratio, and more importantly, an improved sidewall verticality due to the lower aspect ratio of the etched holes. Conical (non-vertical) etching of the holes leads to coupling to leaky TM modes of the slab[27], which eventually decreases the Q.

Gain–cavity coupling is achieved through directly transferring the WSe_2 monolayer onto the top of the PCC, using methods that are well established for 2D materials. In the cartoon plot of Fig. 1a, we show the electric-field intensity profile (x–y plane) of the fundamental mode defined by our cavity, simulated by the finite-difference time-domain (FDTD) method[23]. Figure 1d illustrates the cross-section (x–z plane) profile of the mode, where the orange dashed line indicates the ideal position of WSe_2 monolayer. The corresponding electric-field intensity at the monolayer is about 40% of the possible maximum (which is located at the centre), allowing for efficient overlap between the cavity mode and the monolayer WSe_2 on the surface. In our geometry, even though the gain medium is placed outside the cavity, the miniaturization of the monolayer (with a thickness of ~0.7 nm) allows minimal degradation of gain–cavity coupling.

Lasing at a reduced threshold power is achieved by enhancing spontaneous emission into a resonant cavity mode. Figure 1e shows a typical emission spectrum of the hybrid structure, taken under optical pumping by a 632 nm continuous-wave (CW) laser at 80 K. The laser emission is the sharp feature located at 739.7 nm; we measure a line width of 0.3 nm at the half-maximum of this spectrum. The peak is polarized in the y direction, consistent with the fundamental mode of the cavity.

One hallmark feature of a laser is the nonlinear 'kink' that occurs around the lasing threshold in the log scale plot of the output light intensity (detected power obtained by integrating over the spectrum) as a function of incident pump power (the 'light–light', or L–L, curve). In Fig. 2a, b, we present the L–L curves (red filled squares) for the monolayer laser at temperatures of 130 K and 80 K, respectively; both curves show the nonlinear 'kink' at the laser threshold region. We estimate typical emission power levels (after the objective lens) of our lasing devices in this region to be ~10 fW with 100 nW incident pump power. A set of power-dependent data for spontaneous emission off cavity resonance is also shown in Fig. 2a for contrast (violet half-filled squares); no 'kink' signature is observed. The photoluminescence spectra corresponding to the denoted data points (arrows in Fig. 2b) are shown in Fig. 2c. The L–L curve in Fig. 2a is fitted by the cavity laser rate equation (see Methods), as shown by the solid lines.

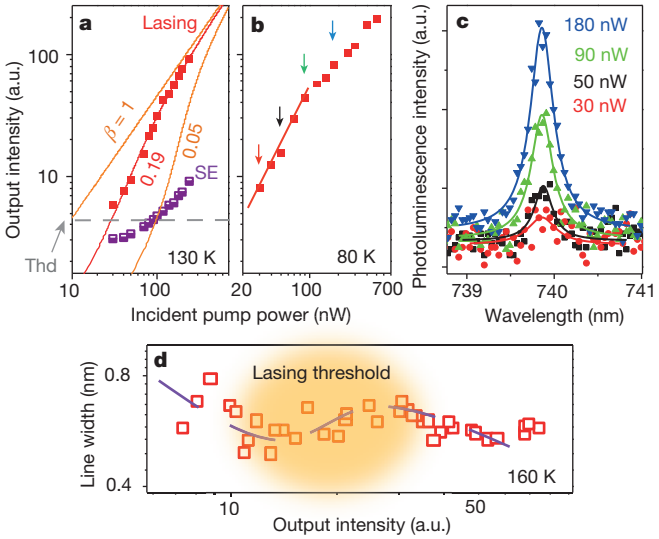

Figure 2 | Lasing characteristics. **a**, Light output intensity (detected power after spectrometer) as a function of the optical pump power (L–L curve) at 130 K. Red filled squares correspond to the cavity emission. Violet half-filled squares correspond to the spontaneous emission (SE) off cavity resonance. Solid lines are the simulated curves using the laser rate equation with different β-factors. $\beta = 0.19$ is the best fit to the lasing data. Dark grey dashed line corresponds to the defined laser threshold, labelled by 'Thd'. **b**, L–L curve for the same lasing device at 80 K (red squares), where the solid line is a guide for the eye to the transition region. **c**, The photoluminescence spectra corresponding to the data points in **b** indicated by the coloured arrows. The solid lines are Lorentzian fits to the photoluminescence spectra. **d**, Cavity line width as a function of the detected output power at 160 K (open red squares). See Extended Data Fig. 3 for the line width at 80 K. Dashed line is a guide to the eye to the nonlinear line width re-broadening area, which corresponds to the lasing threshold region. a.u., arbitrary units.

In a nanocavity laser, the β-factor is the figure of merit that characterizes the laser threshold, and is defined as the fraction of spontaneous emission into the cavity mode (see Methods). A large β-factor reduces the lasing threshold power. We find that $\beta = 0.19$ is the best fit to our observed data, while $\beta = 0.05$ and $\beta = 1$ are also plotted in Fig. 2a for reference. This indicates that in our WSe_2–cavity system, about 19% of the total spontaneous emission is coupled to the cavity mode, comparable to the performance achieved in quantum-dot photonic crystal cavity lasers. We calculate the lasing threshold of our device to be 27 nW (~1 W cm^{-2}), as measured by the incident power. Such ultralow-threshold lasing behaviour demonstrates that the cavity–gain coupling in the surface-gain geometry is as efficient as that in the embedded quantum-dot structure[6,7].

The observed ultralow lasing threshold relies on the high-Q cavity mode. This assertion can be further supported by the data taken from the same device with a lowered Q-factor, achieved by covering the device with a poly(methyl methacrylate) (PMMA) layer on top. In this situation, the lasing threshold increases up to around 100 μW (Extended Data Fig. 2).

We also study the line width evolution around the lasing threshold region. Figure 2d shows the line width as a function of output intensity at 160 K. A pronounced 'kink' appears around the threshold, similar to that in the L–L curve. Below the threshold, the observed line width narrows from ~0.75 nm to ~0.50 nm as output power increases. At the threshold regime, it broadens to ~0.65 nm, and then continues to narrow to 0.55 nm. This line width-dependence is a well-known feature that has been observed in semiconductor nanocavity lasers, such as quantum-well[28] and quantum-dot nanolasers[7]. The 'kink' arises during the phase transition from spontaneous emission into stimulated emission, where the coupling between intensity and phase noise (gain–refractive index coupling) significantly

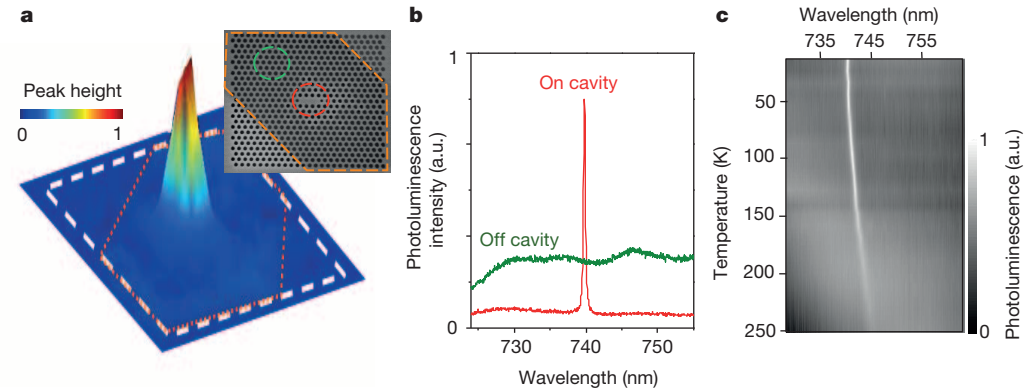

Figure 3 | Spatially resolved emission and temperature-dependent device behaviour. **a**, Peak distinguishing spatial map of our device, where peak height—that is, normalized intensity difference between peak summit (739.7 nm) and bottom (738 nm), is mapped out at 80 K. Dashed white line indicates the photonic crystal area and the dashed orange line shows the area that is covered by monolayer WSe_2. Inset, corresponding device image in SEM. **b**, Photoluminescence spectra taken on (red) and off (green) the cavity region, indicated by the dashed colour circles in **a** inset. **c**, Temperature dependence of the device emission spectra in a grey-scale map.

influences the line width, and leads to a broadened emission spectrum[7,28,29]. Such an observed line width plateau, together with the L–L curve, clearly reveals the lasing behaviour in our monolayer semiconductor nanocavity system.

It is essential to lasing that the cavity mode dominates the emission. To illustrate this, we present a contrast experiment between on- and off-cavity regions, by performing a scanning micro- photoluminescence measurement on our device. In Fig. 3a, we plot a peak distinguishing map, in which the normalized peak height of the lasing spectrum (at 739.7 nm) is mapped out over the entire photonic crystal region, indicated by the dashed white line. The dashed orange line indicates the position of the monolayer WSe_2, as also shown in the inset SEM device image. The laser emission only comes from the cavity. A set of typical spectra taken on and off cavity (indicated by dashed circles in Fig. 3a) is shown in Fig. 3b. The on-cavity emission is dominated by the lasing mode while the non-lasing spontaneous emission is largely suppressed, compared to the off-cavity emission. This is strikingly different from observations of the same type in the low-Q device, in which the on-cavity measurement shows a level of broad emission similar to that found in off-cavity measurements[24,25].

Temperature-dependent emission behaviour of our high-Q device is presented in Fig. 3c. A redshift of the emission wavelength with increasing temperature is consistent with the energy shift of the cavity mode[22]. We have examined lasing characteristics at temperatures below 160 K. As the temperature is increased up to about 250 K, the cavity peak diminishes into the recovered background spontaneous emission. A possible explanation of this could be degradation of the cavity resonance induced by differential thermal expansion between the GaP membrane and the WSe_2 monolayer. Nevertheless, in principle there should be no limitation on increasing the lasing temperature. Further improvement of the Q factor by optimizing cavity design and fabrication procedures would be one way to achieve room-temperature lasing. An alternative way would be to find other monolayers or monolayer heterostructures that emit photons at energies compatible with silicon photonics. We could then use silicon PCCs, which have much higher Q-values than that of GaP.

We finally discuss the reproducibility of our new lasing architecture, based on a monolayer semiconductor and a PCC. It is routine to fabricate multiple PCCs on a single chip, while deterministic multiple-transfer of monolayer semiconductors onto different PCCs can be achieved to make monolayer hybrid devices (Fig. 4a). In Fig. 4b, we present the lasing spectrum taken from three different devices on the same chip under similar conditions. The lasing devices can be robustly reproduced, which suggests that mass production could be achieved, especially if large-area monolayers grown from chemical or physical vapour deposition are used.

Our design demonstrates the possibility of achieving scalable nanolasers using monolayer gain for integrated chip systems. The advantage of such a surface geometry is that the construction of the optical nanocavity and that of the gain material is naturally separated, allowing fabrication of both parts individually at high quality, before their non-destructive and deterministic combination as hybrids. This enables their realistic application in a scalable and designable way, compatible with integrated electronic circuits. Electrically pumped operation and electrostatic tuning of the carrier concentration could also be achieved directly, in contrast to conventional designs. Our monolayer surface-gain geometry presents a versatile lasing technology and an advance relative to quantum-dot nanocavity lasers, with gain material being incorporated after the laser cavity fabrication, which eliminates the degradation of the gain medium during the fabrication process and enables its replacement if needed.

The exotic properties of 2D semiconductors may also lead to other novel devices using our device architecture, such as valley-selective lasers. Moving beyond nanolasers, other on-chip photonic implementations, such as the study of strongly coupled cavity quantum electrodynamics[30],

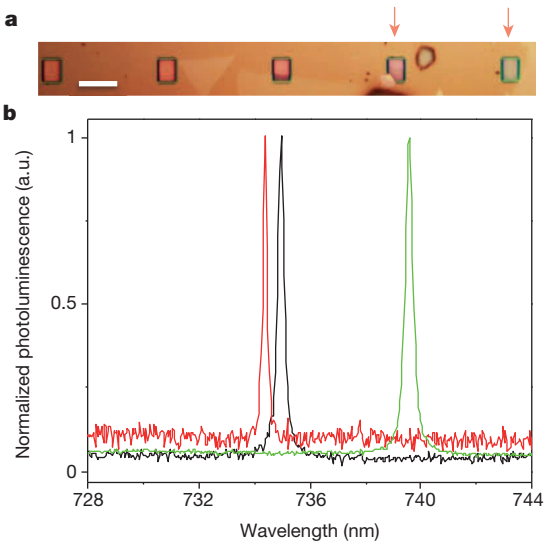

Figure 4 | Reproducibility and scalability of the 2D nanolasers. **a**, An example of deterministic fabrication of multiple devices on one chip. Here we show an optical image of a typical area with 5 PCC devices in a row; the last two devices (indicated by the arrows) are covered with monolayer WSe_2. Scale bar: 10 μm. **b**, Lasing spectra (three) can be reproducibly taken from different devices on the same chip under similar conditions.

nonlinear optics, and photonic quantum control, could open new horizons owing to the use of 2D quantum materials and their heterostructures.

Online Content Methods, along with any additional Extended Data display items and Source Data, are available in the online version of the paper; references unique to these sections appear only in the online paper.

Received 12 October 2014; accepted 3 February 2015.
Published online 16 March 2015.

1. Oulton, R. F. *et al.* Plasmon lasers at deep subwavelength scale. *Nature* **461,** 629–632 (2009).
2. Lu, Y.-J. *et al.* Plasmonic nanolaser using epitaxially grown silver film. *Science* **337,** 450–453 (2012).
3. Painter, O. *et al.* Two-dimensional photonic band-gap defect mode laser. *Science* **284,** 1819–1821 (1999).
4. Khajavikhan, M. *et al.* Thresholdless nanoscale coaxial lasers. *Nature* **482,** 204–207 (2012).
5. Hill, M. T. *et al.* Lasing in metallic-coated nanocavities. *Nature Photon.* **1,** 589–594 (2007).
6. Strauf, S. *et al.* Self-tuned quantum dot gain in photonic crystal lasers. *Phys. Rev. Lett.* **96,** 127404 (2006).
7. Strauf, S. & Jahnke, F. Single quantum dot nanolaser. *Laser Photon. Rev.* **5,** 607–633 (2011).
8. Ellis, B. *et al.* Ultralow-threshold electrically pumped quantum-dot photonic-crystal nanocavity laser. *Nature Photon.* **5,** 297–300 (2011).
9. Mak, K. F., Lee, C., Hone, J., Shan, J. & Heinz, T. F. Atomically thin MoS_2: a new direct-gap semiconductor. *Phys. Rev. Lett.* **105,** 136805 (2010).
10. Splendiani, A. *et al.* Emerging photoluminescence in monolayer MoS_2. *Nano Lett.* **10,** 1271–1275 (2010).
11. Mak, K. F. *et al.* Tightly bound trions in monolayer MoS_2. *Nature Mater.* **12,** 207–211 (2013).
12. Ross, J. S. *et al.* Electrical control of neutral and charged excitons in a monolayer semiconductor. *Nature Commun.* **4,** 1474 (2013).
13. Jones, A. M. *et al.* Optical generation of excitonic valley coherence in monolayer WSe_2. *Nature Nanotechnol.* **8,** 634–638 (2013).
14. Xiao, D., Liu, G.-B., Feng, W., Xu, X. & Yao, W. Coupled spin and valley physics in monolayers of MoS_2 and other group-VI dichalcogenides. *Phys. Rev. Lett.* **108,** 196802 (2012).
15. Xu, X., Yao, W., Xiao, D. & Heinz, T. F. Spin and pseudospins in layered transition metal dichalcogenides. *Nature Phys.* **10,** 343–350 (2014).
16. Radisavljevic, B. & Kis, A. Mobility engineering and a metal-insulator transition in monolayer MoS_2. *Nature Mater.* **12,** 815–820 (2013).
17. Sundaram, R. S. *et al.* Electroluminescence in single layer MoS_2. *Nano Lett.* **13,** 1416–1421 (2013).
18. Baugher, B. W. H., Churchill, H. O. H., Yang, Y. & Jarillo-Herrero, P. Optoelectronic devices based on electrically tunable p-n diodes in a monolayer dichalcogenide. *Nature Nanotechnol.* **9,** 262–267 (2014).
19. Ross, J. S. *et al.* Electrically tunable excitonic light-emitting diodes based on monolayer WSe_2 p-n junctions. *Nature Nanotechnol.* **9,** 268–272 (2014).
20. Pospischil, A., Furchi, M. M. & Mueller, T. Solar-energy conversion and light emission in an atomic monolayer p-n diode. *Nature Nanotechnol.* **9,** 257–261 (2014).
21. Lopez-Sanchez, O., Lembke, D., Kayci, M., Radenovic, A. & Kis, A. Ultrasensitive photodetectors based on monolayer MoS_2. *Nature Nanotechnol.* **8,** 497–501 (2013).
22. Rivoire, K., Faraon, A. & Vuckovic, J. Gallium phosphide photonic crystal nanocavities in the visible. *Appl. Phys. Lett.* **93,** 063103 (2008).
23. Chalcraft, A. R. A. *et al.* Mode structure of the L3 photonic crystal cavity. *Appl. Phys. Lett.* **90,** 241117 (2007).
24. Gan, X. *et al.* Controlling the spontaneous emission rate of monolayer MoS_2 in a photonic crystal nanocavity. *Appl. Phys. Lett.* **103,** 181119 (2013).
25. Wu, S. *et al.* Control of two-dimensional excitonic light emission via photonic crystal. *2D Mater.* **1,** 011001 (2014).
26. Schwarz, S. *et al.* Two-dimensional metal-chalcogenide films in tunable optical microcavities. *Nano Lett.* **14,** 7003–7008 (2014).
27. Tanaka, Y., Asano, T., Akahane, Y., Song, B.-S. & Noda, S. Theoretical investigation of a two-dimensional photonic crystal slab with truncated cone air holes. *Appl. Phys. Lett.* **82,** 1661–1663 (2003).
28. Henry, C. Theory of the linewidth of semiconductor lasers. *Quantum Electron. IEEE J.* **18,** 259–264 (1982).
29. Björk, G., Karlsson, A. & Yamamoto, Y. On the linewidth of microcavity lasers. *Appl. Phys. Lett.* **60,** 304–306 (1992).
30. Liu, X., Galfsky, T., Sun, Z., Xia, F. & Lin, E. Strong light-matter coupling in two-dimensional atomic crystals. Preprint at http://arxiv.org/abs/1406.4826 (2014).

Acknowledgements We thank C. Dodson for helping with reflection measurements of nanocavities. This work was mainly supported by AFOSR (FA9550-14-1-0277). A.M. is supported by NSF-EFRI-1433496. Photonic crystal fabrication was performed in part at the Stanford Nanofabrication Facility of NNIN supported by the NSF under grant no. ECS-9731293, and at the Stanford Nano Center. S.W. was partially supported by the State of Washington through the University of Washington Clean Energy Institute. S.B. and J.V. were supported by the Presidential Early Award for Scientists and Engineers (PECASE) administered through the Office of Naval Research, under grant number N00014-08-1-0561. S.B. was also supported by a Stanford Graduate Fellowship. J.Y. and D.G.M. were supported by US DoE, BES, Materials Sciences and Engineering Division. F.H. acknowledges support from the European Commission (FP7-ICT-2013-613024-GRASP).

Author Contributions X.X. and A.M. conceived the experiments. S.B. and A.M. fabricated and characterized PCCs under the supervision of J.V. S.W. fabricated the hybrid devices and performed the measurements with assistance from J.R.S. and L.F., under the supervision of X.X. S.W., X.X., A.M. and S.B. analysed the data, and acknowledge discussions with W.Y. and J.V. J.Y. and D.G.M. provided the bulk WSe_2. F.H. grew the GaP membrane. S.W. wrote the paper with input from all authors.

Author Information Reprints and permissions information is available at www.nature.com/reprints. The authors declare no competing financial interests. Readers are welcome to comment on the online version of the paper. Correspondence and requests for materials should be addressed to X.X. (xuxd@uw.edu) or A.M. (arka@uw.edu).

METHODS

Purcell factor estimation. We estimate the maximum achievable Purcell factor of the cavity, that is, the peak enhancement of the emission rate, through:

$$F_{\max} = \frac{3}{4\pi^2}\frac{Q}{V}\left(\frac{\lambda_c}{n}\right)^3$$

Here $F_{\max}$ is the maximum Purcell factor, Q is the cavity quality factor, $V \approx \left(\frac{\lambda_c}{n}\right)^3$ is the mode volume, $n \approx 3.1$ is the GaP refractive index and $\lambda_c \approx 740$ nm is the cavity emission wavelength. We obtain $F_{\max} \approx 607$ for the as-fabricated cavity $Q = 8{,}000$.

The Q-factor can be smaller after the monolayer transfer. At room temperature, the Q-factor measured after monolayer transfer reduces to ~1,300, consistent with the photoluminescence emission at high temperatures. When cooled down to low temperatures, the Q-factor recovers to ~2,500. The spatial displacement (z direction), due to the surface-gain geometry, and the random dipole directions of the emitter could also affect the enhancement of the spontaneous emission rate. Considering these effects, the Purcell factor should be written as:

$$F = F_{\max}|\psi(s)|^2\langle\cos^2\xi\rangle$$

Here $|\psi(s)|^2 = \left|\frac{E(s)}{E_{\max}}\right|^2 \approx 0.4$ is the field intensity ratio (Fig. 1d) between the surface and the central maximum of the cavity, describing the effect of spatial detuning. ξ is the angle between the emitter dipole direction (random in the x–y plane) and the electric field polarization (the y direction); $\langle\cos^2\xi\rangle = \frac{1}{2\pi}\int_0^{2\pi}\cos^2\xi\,\mathrm{d}\xi = \frac{1}{2}$. Therefore we estimate the Purcell factor as $F \approx 37$ for $Q \approx 2{,}500$, where we consider the monolayer exciton that is spectrally tuned on the cavity resonance and located right above the centre of the cavity.

In a real situation, this value could be further reduced. For example, we may also need to consider the spatial displacement of the exciton in lateral directions, which would require knowledge of the in-plane exciton distribution that is as yet unknown. Moreover, spectral fluctuations of the excitonic line width would lead to variation in the Purcell factor over time described by the Lorentzian of the cavity spectrum. However, the spontaneous emission coupling factor β is estimated to be ~0.19 from our measurements (see next section and Fig. 2a), reflecting an efficient Purcell enhancement in this geometry.

Laser rate equation. The spontaneous emission coupling factor β is an essential figure of merit for a nanocavity laser. To extract its value, we use a rate equation[6] model to describe the evolution of carrier (exciton) number N and the cavity photon number P in the monolayer–PCC system:

$$\dot{N} = R_{ex} - \frac{N}{\tau_{SE}} - \frac{aNP}{\tau_{cav}}, \dot{P} = -\frac{P}{t_c} + \Gamma\frac{N}{\tau_{cav}} + \Gamma\frac{aNP}{\tau_{cav}}, \beta = \frac{\tau_{SE}}{\tau_{cav}}$$

Here, R_{ex} is the optical pumping rate, ${\tau_{SE}}^{-1}$ is the total spontaneous emission rate, ${\tau_{cav}}^{-1}$ is the emission rate into the cavity mode, ${t_c}^{-1}$ is the cavity photon decay rate, aNP is the stimulated emission, which is proportional to $N \cdot P$ with coefficient a, and Γ is the cavity confinement factor. We have ignored non-radiative relaxation processes. The rate of non-radiative decay in monolayer semiconductors is currently not known. Any non-radiative decay would induce additional loss, which would result in a larger β factor[31]. The transparent carrier number is set to be zero, since it does not affect the fitting result significantly.

We set $\dot{N} = 0$ and $\dot{P} = 0$ to obtain the steady state solution of the above coupled equations. The solution is: $R_{ex} = \frac{P}{\Gamma t_c(1+aP)}\left(\frac{1}{\beta} + aP\right)$. The lasing threshold is defined as the condition when the stimulated emission is equal to the spontaneous emission in the cavity, that is, $aP = 1$. When $aP > 1$, stimulated emission dominates in the hybrid system and lasing behaviour occurs.

We fit our experimental L–L curve with above equation, as plotted in Fig. 2a. $\beta = 0.19$ is found to be the best fit to the data taken at 130 K.

PCC fabrication. To fabricate the photonic crystal structures, a 125-nm-thick GaP membrane was grown on top of a 1-μm-thick sacrificial $Al_{0.8}Ga_{0.2}P$ layer on a GaP wafer via gas-source molecular beam epitaxy (GSMBE). The patterns were first defined in ZEP520 resist by electron-beam lithography (JEOL JBX 6300, 100 keV) and then transferred to the GaP membrane by a chlorine-based reactive ion etch. Excess resist was removed with Microposit remover 1165 followed by oxygen plasma. The sacrificial layer was finally undercut with hydrofluoric acid to yield suspended membrane structures with high index contrast, followed by cleaning in dilute KOH to remove any by-products of the undercut.

Hybrid device fabrication. The PCC–WSe_2 hybrid structure was fabricated through a standard polymer microtransfer process. A monolayer WSe_2 was first mechanically exfoliated onto a polymer-coated silicon substrate where water-soluble polyvinyl alcohol (PVA, 1%) followed by poly(methyl methacrylate) (PMMA, 950, 6%) was spin-coated on the chip. The stacked monolayer WSe_2/PMMA/PVA/Si substrate was then placed on water, dissolving the PVA layer to separate the silicon substrate. The floating WSe_2/PMMA membrane was transferred using a 'perfect loop' (Ted Pella, Inc.), placing the monolayer onto the pre-fabricated PCC under a microscope followed by heating. The PMMA cover layer was dissolved by a 2-h acetone bath and a 2-min isopropyl alcohol bath.

Sample size. In the above analyses, no statistical methods were used to predetermine sample size.

31. Björk, G., Karlsson, A. & Yamamoto, Y. Definition of a laser threshold. *Phys. Rev. A* **50,** 1675–1680 (1994).

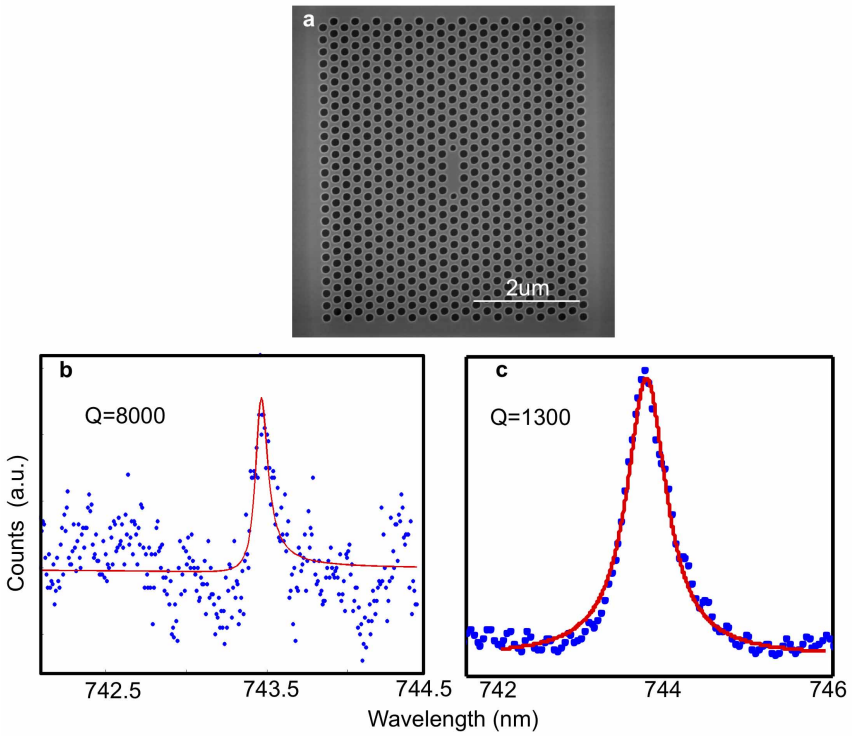

Extended Data Figure 1 | Cavity *Q*-factor determination. **a**, SEM image of a typical PCC. **b, c**, Room-temperature cross-polarized reflection taken from this cavity, before (**b**) and after (**c**) monolayer WSe_2 transfer. As-fabricated cavities (before transfer) of our lasing devices typically have *Q*-factors ranging from 5,000 to 14,000. After monolayer transfer, the *Q*-factor is reduced from 8,000 to 1,300 in this device. After cooling down to cryogenic temperatures, the *Q*-factor recovers to ~2500.

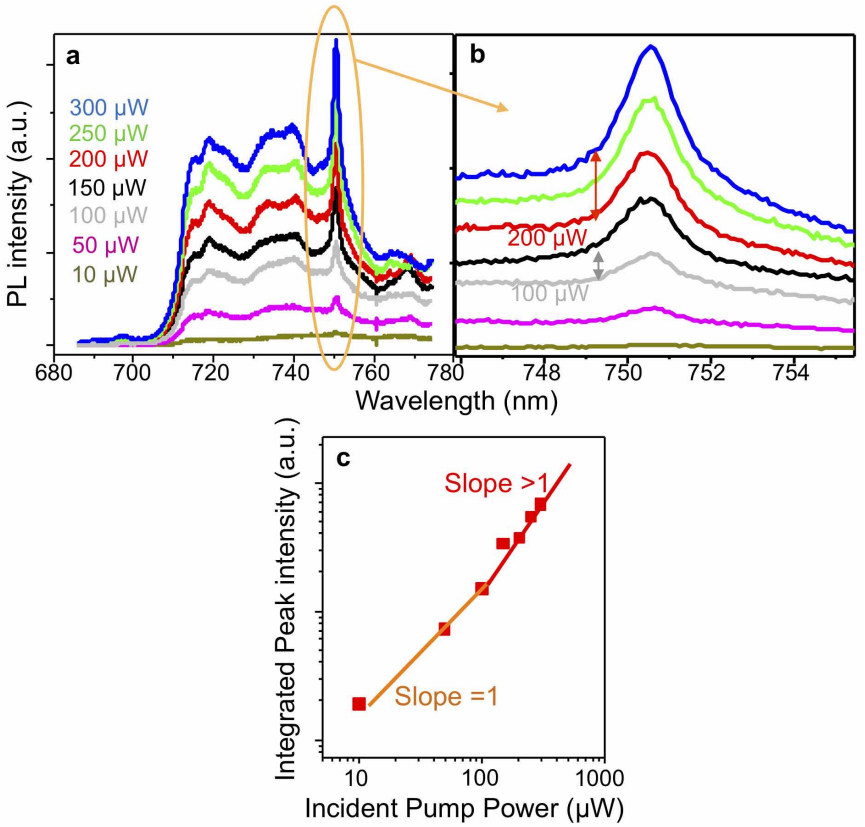

Extended Data Figure 2 | Behaviour of device with *Q*-factor reduced by poly(methyl methacrylate). **a**, Photoluminescence spectra taken from the PMMA covered device at different pumping powers (30 K), showing pronounced cavity peaks. **b**, Magnified view of cavity peaks ringed in **a**. **c**, Power dependence of the integrated peak intensity. A nonlinear 'kink' appears around 100 μW. The PMMA layer reduces the *Q*-factor to ~500, and also shifts the resonance to lower energy (750.7 nm). This supports the conclusion that the ultralow lasing threshold in our device results from the high *Q*-factor, by significantly enhancing the spontaneous emission rate into the lasing mode.

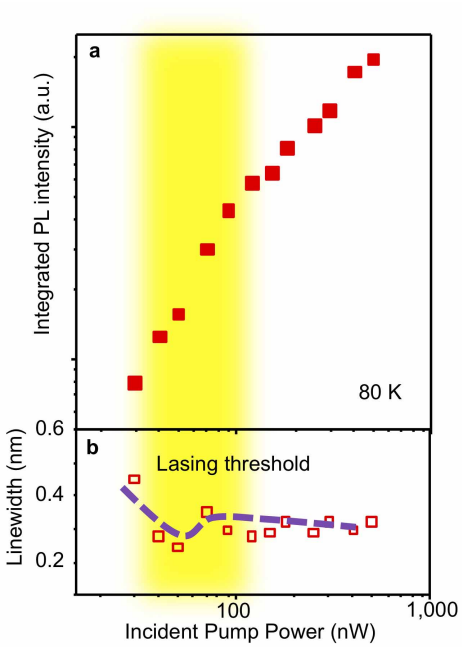

Extended Data Figure 3 | Nonlinear 'kinks' in plots of device properties at 80 K. a, **b**, Plots show pump power dependence of integrated emission intensity (**a**) and line width (**b**). The same set of data are shown here as in Fig. 2b.